

Role of time resolution on polarization of pulsar radiation

R.T. Gangadhara^{1,2,3}, K.M. Xilouris⁴, A. von Hoensbroech³, M. Kramer³, A. Jessner³, and R. Wielebinski³

¹ Indian Institute of Astrophysics, Bangalore-560034, India

² National Centre for Radio Astrophysics, TIFR, Pune University Campus, Pune-411007, India

³ Max-Planck-Institut für Radioastronomie, Auf dem Hügel 69, D-53121 Bonn, Germany

⁴ Cornell University, National Astronomy and Ionospheric Center, Arecibo Observatory, P.O. Box 995, Arecibo, PR 00613, USA

Received 3 May 1998 / Accepted 27 October 1998

Abstract. The role of orthogonal polarization modes in pulsar emission is re-examined in view of polarization data of high time resolution. Individual pulse data of PSR B1133+16 at 1.41 GHz, obtained with time resolutions of 1160, 500 and 150 μ s, were statistically analyzed and the results are presented as probability of occurrence gray-scale maps. Orthogonal modes are recognized in all three data sets, however, they appear better separated in the high resolution data set. Our analysis indicates that the occurrence of these modes is affected by the time resolution of the observation. In the high resolution data, where the modes are better separated, the emission appears highly polarized. We find that the linear polarization becomes higher when the circular polarization is at minimum, an observation which is in agreement with the predictions of curvature emission.

Key words: polarization – stars: pulsars: general – stars: pulsars: individual: PSR B1133+16

1. Introduction

Pulsars are known for about the past three decades, and an enormous amount of effort has been devoted in understanding their emission process. There are models based upon plasma mechanisms (e.g. Asseo et al. 1990), maser mechanisms (e.g. Melrose 1992) and single particle approaches (e.g. Ruderman & Sutherland 1975). Some of them have succeeded in explaining radio pulse intensity, however, the polarization properties of individual pulses are hard to explain in the context of these models. Nevertheless, they do provide a basic understanding of the relevant physical processes.

The importance of polarization in the pulsar radio emission as a signature of emission mechanism is well known. To understand the average polarization angle swing seen in observations of radio pulsars, many attempts have been made to fit the observations with the rotating vector model (RVM) introduced by Radhakrishnan & Cooke (1969). The fits have been very successful in many cases. However, some pulsars do not fit with this interpretation (e.g. Manchester 1971; Rankin, Campbell & Backer 1974) and such discrepancies have been attributed to the occurrence of orthogonal polarization modes (e.g. Backer, Rankin & Campbell 1976; Gil & Lyne 1995; Gangadhara 1997).

It becomes a very difficult task to fit the individual pulse polarization angle swings. The primary (or dominant) polarization mode is consistent with the RVM, and therefore reflects the geometry of magnetic field in the emission region (Gil et al. 1992). The polarization angle swings observed in micropulses and subpulses (Cordes and Hankins 1977) often do not fit with the RVM. As a physical explanation, Gangadhara (1997) has shown that such swings might arise due to the coherent superposition of orthogonal polarization modes.

It is well known that the individual pulses of many pulsars are highly polarized compared to the polarization of the integrated profiles (e.g. Manchester, Taylor & Huguenin 1975). Depolarization (less fractional polarization) is encountered in both average and single pulses, and the reasons given are: (i) propagation effects randomize the polarization angle (Manchester, Taylor & Huguenin 1975) (ii) the subpulse polarization state fluctuates from pulse-to-pulse (Cordes & Hankins 1977), (iii) frequent occurrence of orthogonal jumps (discontinuities of the polarization angle curve) (Lyne, Smith & Graham 1971; Manchester, Taylor & Huguenin 1975; Stinebring et al. 1984a&b; McKinnon & Stinebring 1996), (iv) systematic drift of subpulses (Taylor et al. 1971), (v) incoherent superposition of a large number of elementary emitters from different field lines (Gil, Kijak & Życki 1993) and (vi) intrinsic to the emission process (Xilouris et al. 1994).

With the aim of understanding orthogonal polarization modes, the present work focuses on the role of instrumental time resolution on the polarization angle swing and the depolarization in individual pulses.

2. Observations and data reduction

The pulsar PSR B1133+16 was observed with the 100-m Effelsberg radiotelescope of MPIfR. Observations were made at the center frequency 1.41 GHz with a bandwidth of 40 MHz, using a tunable HEMT-receiver with a system temperature of about 28 K. The two circular polarizations are separated in the receiver and amplified. The signals are then fed into an adding polarimeter, a passive device with four output channels which allows further online signal processing. Using an online dedispersion device, a four unit 60×667 kHz filterbank, the pulse-smearing caused by the dispersion due to the interstellar medium

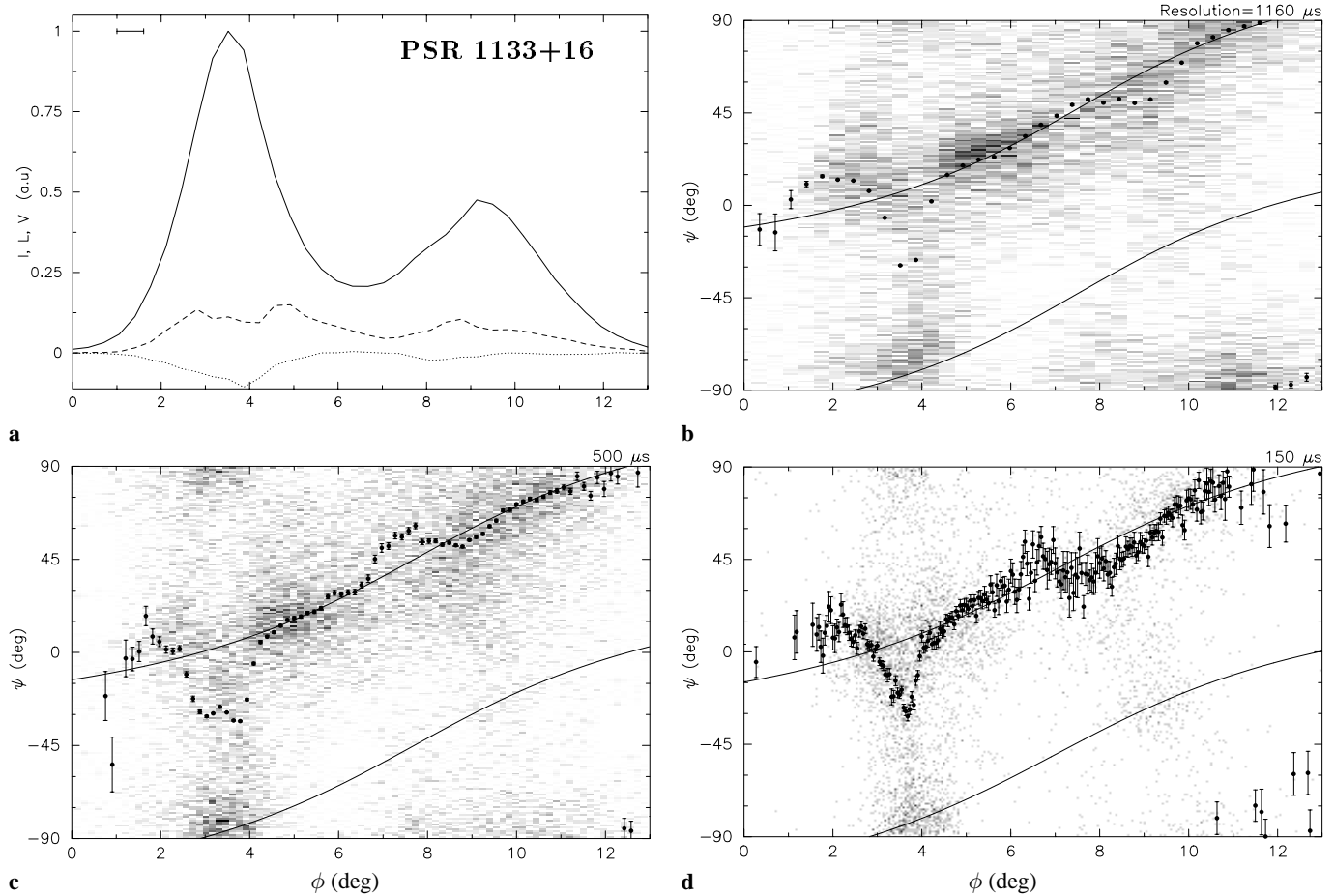


Fig. 1a–d. The average polarization profile of PSR B1133+16 in arbitrary flux units (a.u) and polarization angle (ψ) gray-scale maps. The panels **b**, **c** and **d** represent the polarization angle gray-scale maps obtained from individual pulses with time resolutions of 1160, 500, and 150 μs , respectively. A marker of time duration 2 ms is given at the upper-left corner of panel **a**. The average polarization angle curves and the RVM fits are superposed. The shade is a number in the range 0 (white) and 1 (black) obtained by linear interpolation between the background and foreground levels.

is removed. The output of each channel is then detected and converted into a digital signal by a fast A/D converter. After a time delay according to the dispersion measure, the outputs of all channels are added and then recorded by the backend. After a careful calibration, Stokes parameters are obtained from the four recorded output channels. The system description and the calibration procedure are given by von Hoensbroech & Xilouris (1997).

We recorded three sets of single pulse data (each set containing about 500 individual pulses) with time resolutions of 1160, 500 and 150 μs on three different observing sessions during September 1996. PSR B1133+16 is strong at 1.41 GHz, and has a small dispersion measure ($\text{DM}=4.8 \text{ cm}^{-3} \text{ pc}$), which makes it a good source for studying orthogonal polarization modes with high time resolution. The average polarization parameters: intensity I , linear L and circular V polarization are plotted as a function of pulse phase in Fig. 1a. The continuous line curve indicates I while the broken and dotted ones represent L and V , respectively, in arbitrary units. We do not find any

significant difference between this average profile and the other average profiles obtained from 500 μs and 150 μs time resolutions data. The polarization properties of the average profile, a well-resolved double lobe, show notable differences between the leading component and the rest of the profile. The leading component is only $\sim 10\%$ polarized while the saddle and trailing components are $\sim 20\%$ polarized (Manchester, Taylor & Huguenin 1975; Cordes & Hankins 1977).

2.1. Polarization angle swing of orthogonal modes

The gray-scale maps in Fig. 1b–d show the frequency of occurrence of orthogonal polarization modes with respect to the pulse phase for three different time resolutions. We used the *pgplot* routines developed by Pearson (1989) for making gray-scale maps. The fortran subroutine *pggray* draws gray-scale map of an array in the ψ – ϕ plane, by determining the shade of each point from the corresponding array value. The shade is a number in the range from 0 to 1 obtained by *linear interpolation*

between the background level (white) and the foreground level (black). The white regions in the maps are with shade = 0 and darkest regions are with shade = 1.

This technique has become a powerful tool in analyzing the pulsar polarization properties (e.g. Stinebring et al. 1984a,b). The panels b–d in Fig. 1 represent the polarization angle gray-scale maps at the time resolutions of 1160, 500 and 150 μs , respectively. To compare the three time resolutions we have given a marker of time duration 2 ms at the upper-left corner of Fig. 1a. The darkest shades represent the most probable regions of occurrence. At each pulse phase bin, the full range of polarization angle was divided into 200 intervals. In this way, the gray-scale maps were made from all those phase bins where the linear polarization L is above 4σ level. Here σ is the *rms* of L in the off pulse region. All those phase bins, where the condition $L^2 + V^2 \leq I^2$ was not met, were excluded as they lead to spurious polarization quantities.

The curves represented by points, associated with error bars, indicate the integrated polarization angle swing. They follow closely the mode which is strong at any pulse phase. The RVM was proposed to explain the polarization angle swing in integrated pulse profiles (e.g. Manchester and Taylor 1977):

$$\psi = \arctan\left[\frac{\sin \alpha \sin(\phi - \phi_0)}{\sin \zeta + \sin \alpha \cos(\alpha + \zeta)\{1 - \cos(\phi - \phi_0)\}}\right] + \psi_0, \quad (1)$$

where the parameters are ϕ the rotation phase, α the angle between rotation and magnetic axes, and ζ the impact parameter, i.e., the angle between the magnetic axis and the line-of-sight.

We fitted the function $\psi(\phi, \alpha, \zeta)$ to the observed polarization angle using two different numerical algorithms. First, the robust Simplex Algorithm (Nelder & Mead 1965) was applied to get close to the minimum of χ^2 , and the minimum was then optimized with the Levenberg–Marquardt Algorithm (Marquardt 1963). The goodness of the fit was tested using the classical χ^2 -test and Kolmogorov–Smirnov test (e.g. Press et al. 1992). We found with $\alpha = 88^\circ \pm 5^\circ$ and $\zeta = 7^\circ \pm 2^\circ$ the RVM can be fitted to all three data sets. Using these values α and ζ , the RVM was fitted with the polarization angle swing of orthogonal polarization modes, as indicated by the continuous line curves in Figs. 1b–d.

In Fig. 1b, orthogonal polarization modes appear separated only under the leading component, while under the trailing component one mode has become too weak. In the case of incoherent addition of radiation fields, Stokes parameters become additive (Gangadhara 1997). Therefore, it is the stronger mode, which determines the polarization angle in the case of low resolution observations. In Fig. 1c, orthogonal polarization modes are not clearly seen under the trailing component, as they are not yet fully separated, while in Fig. 1d they are separated in both components.

The gray-scale maps and the integrated polarization angle swings clearly indicate that the discrepancies between the RVM and the polarization angle swing in average pulses arises due to the presence of orthogonal polarization modes. The non-orthogonal (random) radiation, which does not fit with the RVM

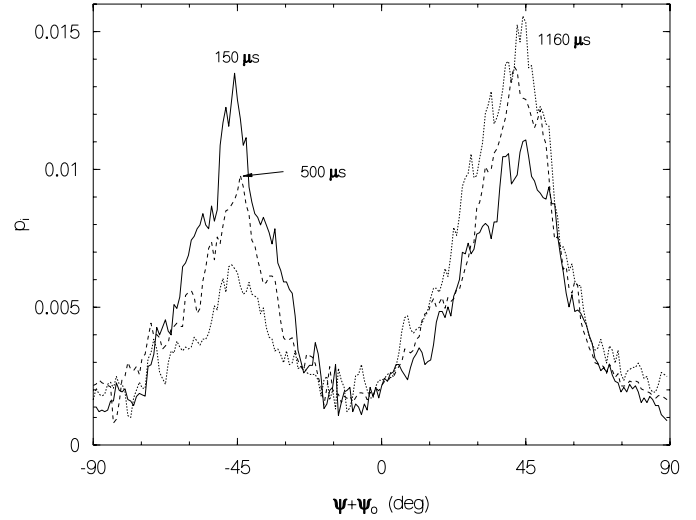


Fig. 2. The probability of occurrence of pulsar radiation at different polarization angles. The dotted, broken and continuous line curves represent the pulses with time resolutions of 1160, 500, and 150 μs , respectively. To display the two humps clearly position angle rotation of $\psi_0 = 40^\circ$ has been applied.

model, exists in all our data sets. The polarization angle closely follows the stronger mode in any phase bin.

To investigate the effect of time resolution on orthogonal polarization modes, we consider the pulse phase between $2^\circ \leq \phi \leq 6^\circ$, where both modes are clearly active. Nearly 15° polarization angle swing over this interval of pulse phase was removed by applying rotation in the opposite direction. Let $i=1, 2, 3, \dots, N$ be the intervals of polarization angle with each one having the width $180/N$. If f_i is the number of pulses (frequency) which appear in the i^{th} interval, then the total number of pulses, which appear in all the N intervals, is given by

$$F = \sum_{i=1}^N f_i. \quad (2)$$

Therefore, the probability of occurrence (relative mode frequency) of pulses in the i^{th} interval is given by

$$p_i = \frac{f_i}{F}, \quad (3)$$

such that the total probability is unity.

Using $N=200$, we computed p_i separately for each data set, and plotted as function of ψ in Fig. 2. The dotted line represents the pulses with 1160 μs resolution, while the dashed and continuous line curves represent the pulses with resolutions of 500 and 150 μs , respectively. Note that we have applied a position angle rotation of 40° while plotting Fig. 2. This rotation was just to make the two humps clearly visible. It can be clearly seen that the polarization angle preferentially occurs around the two angles separated by about 90° . At low resolutions the primary mode, which is at $\psi + \psi_0 \approx 45^\circ$, is observed more often than the secondary mode, which is at $\psi + \psi_0 = -45^\circ$. At the higher resolution, orthogonal polarization modes are better resolved and the probability of observing the secondary mode becomes

comparable to that of primary mode. Hence the probability of detection of orthogonal polarization modes is affected by the data resolution.

2.2. Depolarization

To investigate the role of time resolution on the polarization properties of pulsar radiation, we have analyzed single pulses with different time resolution. We used 4σ threshold on I and L , and considered the full range of pulse phase (13°). The gray-scale maps which represent the correlation between the fractional linear $L(\%) = 100L/I$, and circular $V(\%) = 100V/I$ polarization and I , are shown in Figs. 3 and 4.

When the resolution is high, both linear and circular polarization are also high as indicated by Figs. 3c and 4c. This is because the short time scale structures such as micropulses are often highly polarized, which leads to high polarization when observed with a higher resolution.

Figs. 3a–c indicate the correlation between the linear polarization and circular polarization. It is evident that the linear polarization becomes higher when circular polarization is at minimum. This is in agreement with the predictions of curvature radiation (Gil et al. 1993; Gangadhara 1997). Figs. 4a–c indicate the behaviour of circular polarization with respect to the intensity at different time resolutions. They indicate that at lower intensity and higher resolution, circular polarization is higher.

3. Discussion

In the high resolution observations, orthogonal polarization modes are better resolved and we find them in both (leading and trailing) components of PSR B1133+16 in agreement with results for the same pulsar at 1.4 GHz by Backer & Rankin (1980) and Cordes & Hankins (1977). The polarization display presented by Stinebring et al. (1984a) shows the presence of orthogonal polarization modes in the leading component while in the trailing component they are not clearly resolved.

The polarization angle swing of orthogonal polarization modes has been interpreted as two polarization angle curves, each of which is consistent with the RVM and separated by about 90° (Cordes et al. 1978; Backer & Rankin 1980; Gil & Lyne 1995). If the modes exist disjointly, the polarization angle should follow either one mode or the other. However, Figs. 1b–d show that not all the radiation appears at the two preferred values of polarization angle. We see a significant amount of non-orthogonal radiation in between those preferred values of polarization angle. Similarly, if we compare the polarization angle gray-scale maps of PSR B0834+06 made with resolution of $1240 \mu\text{s}$ at 1.4 GHz (Stinebring et al. 1984b) with another made with resolution of $400 \mu\text{s}$ (Stinebring et al. 1984a), we see the same behaviour. These investigations clearly indicate that the non-orthogonal radiation is affected by the time resolution of observations. The coherent superposition of orthogonal polarization modes can contribute to the non-orthogonal radiation (Gangadhara 1997). Also, the idea that the super-

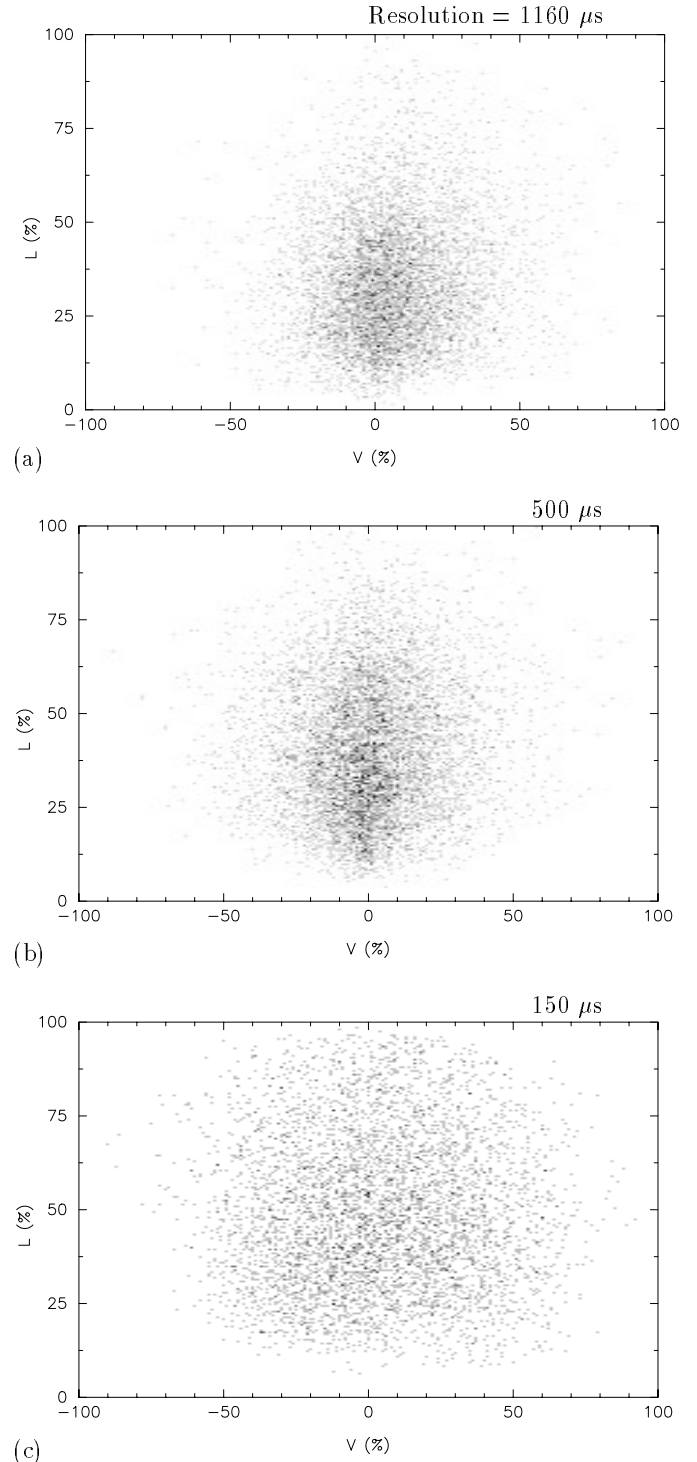


Fig. 3a–c. Grey-scale maps representing the correlation between $L(\%)$ and $V(\%)$ in the individual pulses at resolutions of 1160, 500, and 150 μs . The shade is a number in the range 0 (white) and 1 (black) obtained by linear interpolation between the background and the foreground levels.

position of orthogonal polarization modes is responsible for non-orthogonal radiation is supported by the observation that the non-orthogonal radiation becomes significant only at those

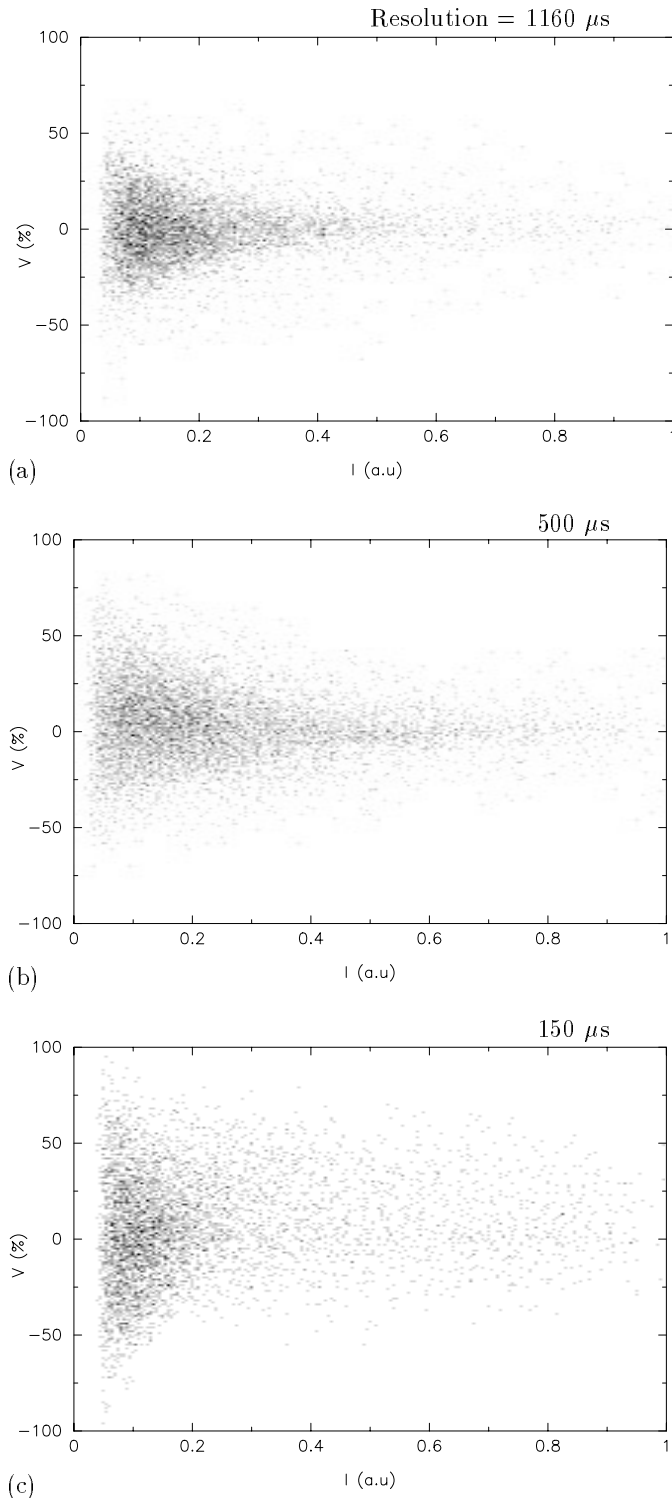


Fig. 4a–c. Grey-scale maps representing the correlation between $V(\%)$ and I in the individual pulses at resolutions of 1160, 500, and 150 μs .

pulse longitudes where both modes exist. For example, see the polarization angle distributions of PSR B0823+26, B0950+08 (Stinebring et al. 1984a), B0834+06 (Stinebring et al. 1984b), and B0329+54 (Gil & Lyne 1995). McKinnon and Stinebring

(1996) have also suggested that the non-orthogonal (uniform or random) radiation may arise from the superposed modes.

If the radiation process has a beam width $\sim 1/\gamma$, where γ is the relativistic Lorentz factor, it can also give a spread in polarization angle when the radiation is received from the field lines which are nearby to the line-of-sight. However, such a spread is too small compared to the instrumental resolution, assuming $\gamma \sim 100$ (Melrose 1992). Manchester, Taylor & Huguenin (1975) have suggested that propagation effects could randomize the polarization angle.

We have demonstrated the role of time resolution on the polarization of radiation by observing at the same frequency with different time resolutions. The micropulses exist throughout the pulse, and they are highly polarized (Cordes & Hankins 1977), therefore, the polarization appears higher in the highest resolution observations. McKinnon and Stinebring (1996) have suggested that pulsars depolarize by superposed orthogonal polarization modes.

4. Conclusion

In the observations of higher time resolution, orthogonal polarization modes are better resolved. The polarization angle of each mode is well described by the RVM as a geometric interpretation. The discrepancy between the RVM and the average polarization angle swing arises due to the presence of orthogonal polarization modes.

We observe that at higher time resolutions both the linear and the circular polarization are high because in such observations the highly polarized and short time scale features such as micropulses are better resolved. The depolarization in the single pulses might be due to the superposition of radiation emitted from different regions separated by distance larger than the wavelength. The high resolution observations and the individual pulse studies are more welcome in understanding the pulsar radio emission. Our result that the linear polarization becomes high when the circular polarization is at minimum favour the predictions of curvature emission.

Acknowledgements. It is pleasure to thank Y. Gupta, D. Lorimer and W. Sieber for interesting discussions and comments on the manuscript. We are grateful to anonymous referee for many useful comments.

References

- Asseo E., Pelletier G., Sol H., 1990, MNRAS 247, 529
- Backer D.C., Rankin J.M., 1980, ApJSS 42, 143
- Backer D.C., Rankin J.M., Campbell D.B., 1976, Nat 263, 202
- Cordes J.M., Hankins T.H., 1977, ApJ 218, 484
- Cordes J.M., Rankin J.M., Backer D.C., 1978, ApJ 223, 219
- Gangadhara R.T., 1997, A&A 327, 155
- Gil J.A., Kijak J., Życki P., 1993, A&A 272, 207
- Gil J.A., Lyne A.G., Rankin J.M., Snakowski J.K., Stinebring D.R., 1992, A&A 255, 181
- Gil J.A., Lyne A.G., 1995, MNRAS 276, L55
- von Hoensbroech A., Xilouris X.M., 1997, A&A 324, 981
- Lyne A.G., Smith F.G., Graham D.A., 1971, MNRAS 153, 337
- Manchester R.N., 1971, ApJS 23, 283

- Manchester R.N., Taylor J.H., 1977, Pulsars. Freeman, San Francisco
- Manchester R.N., Taylor J.H., Huguenin G.R., 1973, ApJ 179, L7
- Manchester R.N., Taylor J.H., Huguenin G.R., 1975, ApJ 196, 83
- Marquardt D.W., 1963, J. Soc. Ind. Appl. Math. 11, 431
- McKinnon M.M., Stinebring D.R., 1996, In: Johnston S., Walker M.A., Bailes M. (eds.) IAU Colloquium 160: Pulsars: Problems & Progress. ASP Conf. Seri. 105, 483
- Melrose D.B., 1992, Phil. Trans. Soc. Lond. A341, 105
- Nelder F.C., Mead R., 1965, Computer Journal 7, 308
- Pearson T. J., 1989, PGLOT Graphics Subroutine Library, Caltech, Pasadena, A-18
- Press W.H., Teukolsky S.A., Vetterling W.T., Flanery B.P., 1992, Numerical Recipes, Cambridge Univ. Press
- Radhakrishnan V., Cooke D.J., 1969, Astrophys. Lett. 3, 225
- Rankin J.M., Campbell D.B., Backer D.C., 1974, ApJ 188, 608
- Ruderman M., Sutherland P., 1975, ApJ 196, 51
- Stinebring D.R., et al., 1984a, ApJS 55, 247
- Stinebring D.R., et al., 1984b, ApJS 55, 279
- Taylor J.H., Huguenin G.R., Hirsch R.M., Manchester R.N., 1971, Ap. Lett 9, 205
- Xilouris K.M., Kramer M., Jessner A., Wielebinski R., 1994, A&A 288, L17